Inorganic Chemistry

Article

pubs.acs.org/IC

Multiple Single-Molecule Magnet Behaviors in Dysprosium Dinuclear Complexes Involving a Multiple Functionalized Tetrathiafulvalene-Based Ligand

Min Feng, Fabrice Pointillart,* Bertrand Lefeuvre, Vincent Dorcet, Stéphane Golhen, Olivier Cador, and Lahcène Ouahab

Institut des Sciences Chimiques de Rennes UMR 6226 CNRS-UR1, Université de Rennes 1, 35042 Rennes Cedex, France

Supporting Information

ABSTRACT: The reaction between the 2-(1-(2,6-di(pyrazol-1-yl)-4-methylpyridyl)-4,5-(4,5-bis(propylthio)-tetrathiafulvalenyl)-1*H*-benzimidazol-2-yl)-pyridine ligand (**L**) and 2 equiv of $Dy(hfac)_3{\cdot}2H_2O$ ($hfac^-$ = 1,1,1,5,5,5-hexafluoroacetylacetonate) and 1 equiv each of $Dy(hfac)_3{\cdot}2H_2O$ and $Dy(tta)_3{\cdot}2H_2O$ (tta^- = 2-thenoyltrifluoroacetonate) metallic precursors leads to two dinuclear complexes, $[Dy_2(hfac)_6(\mathbf{L})]{\cdot}(CH_2Cl_2)_2{\cdot}C_6H_{14}$ (**1**) and $[Dy_2(hfac)_3(tta)_3(\mathbf{L})]$ (**2**), respectively. Their X-ray structures reveal that the two coordination sites are occupied by one Dy^{III} ion. The Dy^{III} ion coordinated to the benzoimidazolylpyridine (bzip) moiety adopts a D_{4d} coordination sphere, while the Dy^{III} ion coordinated to the 2,6-di(pyrazol-1-yl)-4-pyridine (dpp) moiety is in a D_{3h} surrounding. In a zero dc field, the dynamic magnetic measurements show a slow relaxation for the D_{4d} eight-coordination Dy^{III} magnetization for **1** and **2**. Application of an external dc field induces multirelaxation signals of the magnetic susceptibility for both compounds. The low frequency and high frequency of the out-of-phase magnetic signals are attributed to the Dy^{III} ion in D_{4d} and D_{3h} surroundings, respectively. The two complexes can be described as double induced-field mononuclear single-molecule magnets.

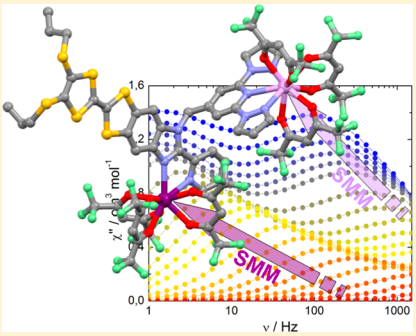

INTRODUCTION

In the molecular magnetism field of research, the lanthanide ions occupy a preponderant place because of their magnetic and luminescence properties. Indeed, their strong single-ion anisotropy and large magnetic moment make them promising candidates for the elaboration of single-molecule magnets (SMMs).[1] The interest in such molecular systems exists because of their abilities to act as a storage unit and to behave as a quantum object, leading to potential applications ranging from high-density data storage devices, spintronics, and quantum computing.[2] SMM behavior can be observed for a single lanthanide complex using a plethora of organic ligands such as the main known compounds 1,4,7,10-tetraazacyclododecane-*N*,*N*′,*N*″,*N*‴-tetraacetic acid,[3] organometallic sandwich ligand,[4] and phthalocyaninate.[5] In all these systems, the desired axial magnetic anisotropy (Ising anisotropy) is assumed by the ligand because of an adequate charge distribution of the lanthanide surrounding.[6] In the special case of the Dy^{III} ion, a well-known strategy for observing slow magnetic relaxation consists of the coordination of a bis-chelating nitrogenated ligand with a $Dy(\beta\text{-diketonate})_3$ precursor.[7] Using this approach, we proposed to go a step forward in functionalizing the bis-chelating nitrogenated ligand (benzoimidazolylpyridine) with a tetrathiafulvalene (TTF) moiety.[8] The insertion of the TTF fragment guarantees the presence of strong intraligand charge transfer absorption bands for sensitizing the lanthanide luminescence and performing magneto-structural correlation.[9]

In our previous work using 4,5-bis(propylthio)-tetrathiafulvalene-2-(2-pyridyl)benzimidazole-methyl-2-pyridine ligand (**L**′), the amine was alkylated with a methyl-2-pyridine group that is not suitable for the coordination reaction with metallic precursors. Thus, we propose to replace the 2-pyridine fragment with the 2,6-di(pyrazol-1-yl)-4-pyridine (dpp) fragment. In fact, this kind of ligand is suitable for a wide range of physical properties such as those of spin crossover (SCO) complexes,[10] light-induced excited spin state trapping (LIESST) effects,[10a] and luminescent properties,[11] especially in the case of two-photon excitation.[12] Recently, we associated the dpp acceptor with a TTF fragment and studied the magnetic and near-infrared luminescence properties of the resulting lanthanide complexes.[13]

Along these lines, the coordination reactions of $Dy(\beta\text{-diketonate})_3{\cdot}2H_2O$ (β-diketonate = 1,1,1,5,5,5-hexafluoroacetylacetonate ($hfac^-$) and 2-thenoyltrifluoroacetonate (tta^-)) with the ligand 2-(1-(2,6-di(pyrazol-1-yl)-4-methylpyridyl)-4,5-(4,5-bis(propylthio)-tetrathiafulvalenyl)-1*H*-benzimidazol-2-yl)-pyridine (**L**) are presented and X-ray structures of $[Dy_2(hfac)_6(\mathbf{L})]{\cdot}(CH_2Cl_2)_2{\cdot}C_6H_{14}$ (**1**) and $[Dy_2(hfac)_3(tta)_3(\mathbf{L})]$ (**2**) described. The static and dynamic magnetic properties are presented.

Received: February 5, 2015
Published: April 1, 2015

DOI: 10.1021/acs.inorgchem.5b00272
Inorg. Chem. 2015, 54, 4021−4028

EXPERIMENTAL SECTION

Synthesis. *General Procedures and Materials.* The precursors $Dy(hfac)_3{\cdot}2H_2O$ ($hfac^-$ = 1,1,1,5,5,5-hexafluoroacetylacetonate anion) and $Dy(tta)_3{\cdot}2H_2O$ (tta^- = 2-thenoyltrifluoroacetonate anion) were synthesized following previously reported methods.[14] All other reagents were purchased from Aldrich Co., Ltd., and used without further purification.

Synthesis of the Ligand 2-(1-(2,6-Di(pyrazol-1-yl)-4-methylpyridyl)-4,5-(4,5-bis(propylthio)-tetrathiafulvalenyl)-1H-benzimidazol-2-yl)-pyridine (L). A total of 288 mg of 2-(4,5-(4,5-bis(propylthio)-tetrathiafulvalenyl)-1*H*-benzimidazol-2-yl)-pyridine[15] (0.555 mmol) and 116 mg of K_2CO_3 (0.841 mmol, 1.5 equiv) were added to 5 mL of DMF, and then the mixture was stirred for 30 min under argon. A solution of 2 mL of DMF containing 210 mg of 2,6-di(pyrazol-1-yl)-4-(bromomethyl)pyridine[16] (0.692 mmol, 1.25 equiv) was added, and the resulting mixture was heated at 70 °C. After the mixture had been heated for 2 h, additional K_2CO_3 (116 mg, 0.841 mmol, 1.5 equiv) and 2,6-di(pyrazol-1-yl)-4-(bromomethyl)pyridine (100 mg, 0.329 mmol, 0.6 equiv) were added. The mixture was stirred and heated overnight. The bright orange precipitate was filtered, washed with water (3 × 50 mL), and finally dried in air. Yield: 275 mg (67%). Anal. Calcd (%) for $C_{34}H_{30}N_8S_6$: C, 54.99; H, 4.04; N, 15.09. Found: C, 54.74; H, 4.16; N, 15.01. IR (KBr): 2958 (w), 2926 (w), 2870 (w), 2852 (w), 1618 (s), 1571 (m), 1522 (m), 1465 (s), 1396 (m), 1320 (m), 1205 (m), 1041 (m), 954 (w), 859 (w), 782 (w), 751 (m), 608 (w) cm^{-1}. ^1H NMR ($CDCl_3$): δ 8.55 (d, 4.5 Hz, 1H, N), 8.52 (d, 2.3 Hz, 2H, M), 8.46 (d, 8.0 Hz, 1H, L), 7.83 (td, 1.4 Hz, 7.9 and 7.9 Hz, 1H, K), 7.71 (s, 1H, J), 7.69 (s, 2H, I), 7.63 (s, 2H, H), 7.29 (dd, 5.3 and 6.9 Hz, 1H, G), 7.15 (s, 1H, F), 6.46 (s, 2H, E), 6.26 (s, 2H, D), 2.79 (dt, 7.3 Hz, 7.3 and 11.9 Hz, 4H, C), 1.66 (tt, 7.3 Hz, 7.3 Hz, 14.8 and 14.8 Hz, 4H, B), 1.00 (dd, 7.5 and 15.9 Hz, 6H, A).

Synthesis of Complexes 1 and 2. *$[Dy_2(hfac)_6(L)]{\cdot}(CH_2Cl_2)_2{\cdot}C_6H_{14}$ (1).* A total of 32.8 mg of $Dy(hfac)_3{\cdot}2H_2O$ (0.0400 mmol) was dissolved in 10 mL of CH_2Cl_2, and then the mixture was added to a solution of 10 mL of CH_2Cl_2 containing 14.8 mg of **L** (0.0199 mmol). After the mixture had been stirred for 15 min, 25 mL of *n*-hexane was layered at room temperature in the dark. Slow diffusion leads to dark red single crystals that are suitable for X-ray studies. Yield: 44 mg (87%). Anal. Calcd (%) for $C_{72}H_{54}Cl_4Dy_2F_{36}N_8O_{12}S_6$: C, 33.67; H, 2.10; N, 4.36. Found: C, 33.99; H, 2.06; N, 4.61. IR (KBr): 2956 (w), 2928 (w), 2870 (w), 2851 (w), 1653 (s), 1576 (m), 1559 (m), 1533 (m), 1506 (m), 1465 (m), 1412 (m), 1256 (s), 1209 (s), 1145 (s), 1100 (w), 1058 (w), 976 (w), 799 (w), 660 (m), 587 (w) cm^{-1}.

$[Dy_2(hfac)_3(tta)_3(L)]$ (2). A total of 16.4 mg of $Dy(hfac)_3{\cdot}2H_2O$ (0.0200 mmol) and 17.2 mg of $Dy(tta)_3{\cdot}2H_2O$ (0.0200 mmol) were dissolved in 10 mL of CH_2Cl_2, and then the mixture was added to a solution of 10 mL of CH_2Cl_2 containing 14.8 mg of **L** (0.0199 mmol). After the mixture had been stirred for 15 min, 25 mL of *n*-hexane was layered at room temperature in the dark. Slow diffusion leads to small red single crystals that are suitable for X-ray studies. Yield: 44 mg (87%). Anal. Calcd (%) for $C_{73}H_{45}Dy_2F_{27}N_8O_{12}S_9$: C, 37.23; H, 1.91; N, 4.76. Found: C, 37.35; H, 2.02; N, 4.69. IR (KBr): 2958 (w), 2929 (w), 2872 (w), 2850 (w), 1653 (s), 1604 (s), 1540 (s), 1507 (m), 1412 (s), 1309 (s), 1254 (s), 1198 (s), 1144 (s), 792 (m), 661 (m), 585 (m) cm^{-1}.

Crystallography. Single crystals of **1** and **2** were mounted on an APEXII Bruker-AXS diffractometer for data collection (Mo Kα radiation source, λ = 0.71073 Å), from the Centre de Diffractométrie (CDIFX), Université de Rennes 1. Structures were determined with a direct method using the SIR-97 program and refined with a full matrix least-squares method on F^2 using SHELXL-97[17] for **1** and **2**. For **2**, the final data set was made from two measurements as the completeness was not reached with only one. The data sets were scaled and concatenated with the help of JANA2006.[18] Finally, a SQUEEZE procedure of PLATON[19] was performed as this structure contains large solvent accessible voids in which residual peaks of diffraction were observed. Crystallographic data are summarized in Table 1. Complete crystal structure results as a CIF file, including bond lengths, angles, and atomic coordinates, are deposited as Supporting Information.

Table 1. X-ray Crystallographic Data for 1 and 2

	$[Dy_2(hfac)_6(L)]{\cdot}(CH_2Cl_2)_2{\cdot}C_6H_{14}$ (**1**)	$[Dy_2(hfac)_3(tta)_3(L)]$ (**2**)
formula	$C_{72}H_{54}Cl_4Dy_2F_{36}N_8O_{12}S_6$	$C_{73}H_{45}Dy_2F_{27}N_8O_{12}S_9$
M (g mol^{-1})	2566.4	2352.7
crystal system	monoclinic	triclinic
space group	$P2_1/n$ (No. 14)	$P\bar{1}$ (No. 2)
cell parameters	a = 22.3718(12) Å	a = 10.1741(10) Å
	b = 12.6951(6) Å	b = 16.2957(13) Å
	c = 33.6565(19) Å	c = 30.8760(30) Å
	β = 100.859(2)°	α = 98.035(3)°
		β = 90.869(3)°
		γ = 104.958(4)°
volume (Å^3)	9387.7(9)	4889.9(8)
Z	4	2
T (K)	150(2)	150(2)
2θ range (deg)	$5.88 \le 2\theta \le 54.96$	$5.76 \le 2\theta \le 55.96$
ρ_{calc} (g cm^{-3})	1.816	1.598
μ (mm^{-1})	1.956	1.816
no. of reflections	83625	69638
no. of independent reflections	21478	22430
R_{int}	0.0959	0.2259
$F_o^2 > 2\sigma(F_o)^2$	14536	8105
no. of variables	1193	1054
R_1, wR_2	0.1015, 0.2307	0.1112, 0.2606

Physical Measurements. The elementary analyses of the compounds were performed at the Centre Régional de Mesures Physiques de l'Ouest (Rennes, France). ^1H NMR data were recorded on a Bruker Ascend 400 spectrometer. Chemical shifts are reported in parts per million referenced to TMS for ^1H NMR. Cyclic voltametry was conducted in a CH_2Cl_2 solution, containing 0.1 M $N(C_4H_9)_4PF_6$ as the supporting electrolyte. Voltammograms were recorded at 100 mV s^{-1} at a platinum disk electrode. The potentials were measured versus a saturated calomel electrode (SCE). The dc magnetic susceptibility measurements were performed on a solid polycrystalline sample with a Quantum Design MPMS-XL SQUID magnetometer between 2 and 300 K in applied magnetic fields of 0.2 T at 2−20 K and 1 T at 20−300 K. These measurements were all corrected for the diamagnetic contribution as calculated with Pascal's constants.

RESULTS AND DISCUSSION

Synthesis. The target ligand **L** (Scheme 1) was prepared by alkylation of the 2-(4,5-(4,5-bis(propylthio)-tetrathiafulvalenyl)-1*H*-benzimidazol-2-yl)-pyridine[15] with 2,6-di(pyrazol-1-yl)-4-(bromomethyl)pyridine[16] in DMF solvent in good yield.

Scheme 1. Chemical Structure of L with Its Proton Assignments

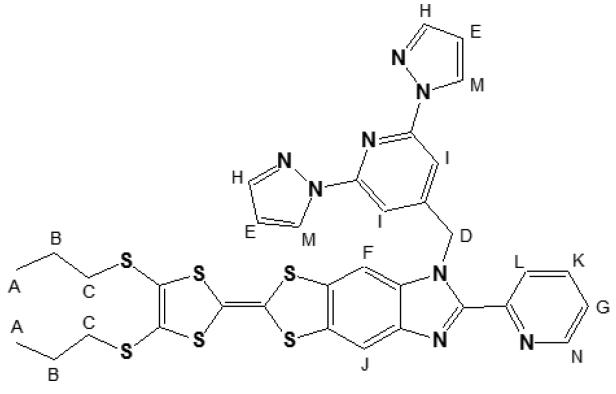

DOI: 10.1021/acs.inorgchem.5b00272
Inorg. Chem. 2015, 54, 4021−4028

Crystal Structures. *[$Dy_2(hfac)_6(L)]\cdot(CH_2Cl_2)_2\cdot C_6H_{14}$ (1).* Compound **1** crystallizes in the $P2_1/n$ (No. 14) monoclinic space group (Table 1). The asymmetric unit is composed of two $Dy(hfac)_3$ moieties, one **L** ligand, two dichloromethane molecules, and one *n*-hexane molecule of crystallization (Figure 1). An ORTEP view is depicted in Figure S1 of the Supporting Information.

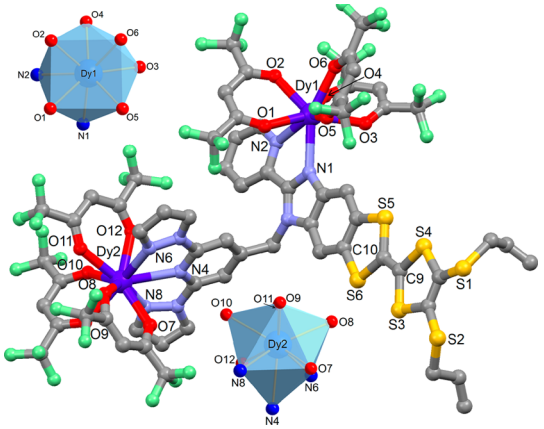

Figure 1. Molecular structure of the dinuclear complex $[Dy_2(hfac)_6(L)]\cdot(CH_2Cl_2)_2\cdot C_6H_{14}$ (**1**) with the coordination polyhedra for both Dy1 and Dy2 ions. Hydrogen atoms and crystallization molecules have been omitted for the sake of clarity.

The X-ray structure reveals that the two coordination sites of **L** are coordinated by $Dy(hfac)_3$ moieties. The Dy1 ion is surrounded by six oxygen atoms that belong to three $hfac^-$ ligands and two nitrogen atoms coming from the bis-chelating coordination site of **L**. The average Dy−O distances are shorter [2.340(8) Å] than the average Dy−N distances [2.527(9) Å] (Table 2) because of the oxophilic character of the lanthanide as usually observed. The arrangement of the ligands leads to a square antiprism (D_{4d} symmetry) as a coordination polyhedron for this dysprosium ion (Table 3). The distortion is visualized by continuous shape measures performed with SHAPE 2.1.[20] The Dy1 coordination polyhedron in **1** is slightly more symmetric than in $[Ln(hfac)_3(L')]$ (where Ln = Dy and Yb and **L′** = 2-{1-methylpyridyl-4,5-[4,5-bis(propylthio)-tetrathiafulvalenyl]-1*H*-benzimidazol-2-yl}pyridine).[8a,9a] The Dy2 ion is surrounded by six oxygen atoms that belong to three $hfac^-$ ligands and three nitrogen atoms coming from the tris-chelating coordination site of **L**. Once again, the average Dy−O distances are shorter [2.361(9) Å] than the average Dy−N distances [2.523(10) Å] (Table 2). The arrangement of the ligands leads to a spherical tricapped trigonal prism (D_{3h} symmetry) as a coordination polyhedron for this dysprosium ion (Table 3). This coordination polyhedron is similar to that observed in the $[Dy_2(hfac)_6(L'')]\cdot C_6H_{14}$ compound (where **L″** = bis(2,6-di(pyrazol-1-yl)-4-methylthiolpyridine)-4′,5′-ethylenedithiotetrathiafulvene).[13] The Dy2−O bond lengths are slightly longer than the Dy1−O ones because of the more bulky 2,6-di(pyrazol-1-yl)-4-pyridine (dpp) acceptor compared to the benzoimidazolylpyridine (bzip) acceptor. The length of the central C=C bond of the TTF core is equal to 1.354(15) Å, which attests to the neutral form of **L**. The two planes formed by the dpp and bzip acceptors are almost perpendicular [88.4(1)°], leading to an intramolecular Dy−Dy distance of 10.85(1) Å.

The shortest S···S contacts are identified as being 3.766(7) Å (S3···S6), 3.885(7) Å (S4···S6), and 3.894(8) Å (S3···S5) and lead to the formation of a dimer of "head-to-tail" donors (space-filling representation in Figure 2). Each dimer is well isolated by the $Dy(hfac)_3$ moieties (ball and stick representation in Figure 2). The shortest intermolecular Dy−Dy distances are equal to 9.669(10) Å (Dy2···Dy2) and 10.117(10) Å (Dy1···Dy1).

[$Dy_2(hfac)_3(tta)_3(L)$] (2). It crystallizes in the $P\bar{1}$ (No. 2) triclinic space group (Table 1). The asymmetric unit is composed of one $[Dy(tta)_2(hfac)]$, one $[Dy(tta)(hfac)_2]$, and one **L** ligand (Figure 3). An ORTEP view is depicted in Figure S2 of the Supporting Information.

The Dy1 ion is surrounded by six oxygen atoms [average distances equal to 2.331(10) Å] that belong to two tta^- ligands, one $hfac^-$ ligand, and two nitrogen atoms [average distances equal to 2.541(12) Å] coming from the bis-chelating bzip moiety of ligand **L**. The Dy2 ion is surrounded by six oxygen atoms [average distances equal to 2.372(10) Å] that belong to one tta^- ligand, two $hfac^-$ ligands, and three nitrogen atoms [average distances equal to 2.535(11) Å] coming from the tris-chelating dpp moiety of ligand **L**. At this point, one remark can be written: to obtain compound **2**, the starting metallic precursors are 1 equiv of $Dy(hfac)_3$ and 1 equiv of $Dy(tta)_3$, but surprisingly, these two metallic fragments are not identified in the X-ray structure. In fact, an exchange between one $hfac^-$ and one tta^- is observed, leading to the coordination of two new metallic $Dy(hfac)_2(tta)$ and $Dy(hfac)(tta)_2$ fragments. This exchange could permit the imposition of a perfect match between the size of the metallic precursors and the coordination sites, leading to a minimum of steric hindrance. SHAPE 2.1 highlights a more distorted square antiprism (D_{4d} symmetry) for the polyhedron of Dy1 in **2** than in **1**, while the coordination polyhedron of Dy2 remains quasi identical with a spherical tricapped trigonal prism (D_{3h} symmetry). The length of the central C=C bond of the TTF core is equal to 1.324(19) Å that attests the neutral form of **L**. The angle between the two dpp and bzip acceptors remains close to orthogonality with a value of 87.8(2)°, leading to an intramolecular Dy−Dy distance of 10.32(1) Å, which is comparable to that measured in **1**.

Table 2. Selected Bond Lengths for Compounds 1 and 2

	1	2
Dy1−O1	2.335(8)	2.311(10)
Dy1−O2	2.311(8)	2.382(11)
Dy1−O3	2.349(8)	2.318(10)
Dy1−O4	2.362(8)	2.328(10)
Dy1−O5	2.345(8)	2.290(9)
Dy1−O6	2.336(9)	2.354(9)
Dy1−N1	2.491(9)	2.502(12)
Dy1−N2	2.563(9)	2.580(11)
Dy2−O7	2.363(9)	2.317(11)
Dy2−O8	2.359(9)	2.343(11)
Dy2−O9	2.322(9)	2.373(9)
Dy2−O10	2.405(9)	2.446(8)
Dy2−O11	2.316(9)	2.398(11)
Dy2−O12	2.402(8)	2.354(10)
Dy2−N4	2.588(9)	2.591(9)
Dy2−N6	2.496(10)	2.521(12)
Dy2−N8	2.486(10)	2.493(12)

DOI: 10.1021/acs.inorgchem.5b00272
Inorg. Chem. 2015, 54, 4021−4028

Table 3. SHAPE Analysis of the Coordination Polyhedra around the Lanthanide in Complexes 1 and 2

	metal	$CShM_{SAPR-8}$ (square antiprism D_{4d})	$CShM_{BTPR-8}$ (biaugmented trigonal prism C_{2v})	$CShM_{TDD-8}$ (triangular dodecahedron D_{2d})	$CShM_{TCTPR-9}$ (spherical tricapped trigonal prism D_{3h})	$CShM_{CSAPR-9}$ (spherical capped square antiprism C_{4v})
1	Dy1	0.435	2.465	2.838	–	–
	Dy2	–	–	–	0.586	0.980
2	Dy1	0.944	1.728	2.004	–	–
	Dy2	–	–	–	0.483	0.831

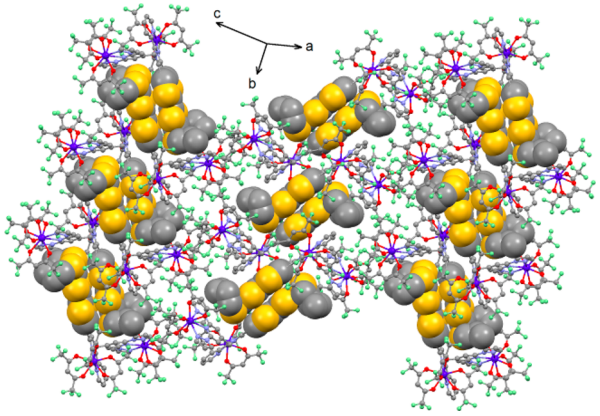

Figure 2. Crystal packing of 1 highlighting the formation of dimers of L.

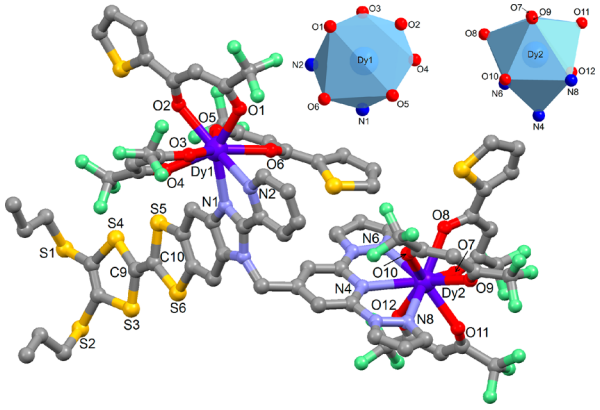

Figure 3. Molecular structure of the dinuclear complex $[Dy_2(hfac)_3(tta)_3(L)]$ (2) with the coordination polyhedra for both Dy1 and Dy2 ions. Hydrogen atoms have been omitted for the sake of clarity.

The shortest S···S contacts are equal to 3.631(7) Å (S4···S6), 3.694(8) Å (S3···S4), and 3.725(8) Å (S3···S5) and lead to the formation of dimer of "head-to-tail" donors (space-filling representation in Figure 4). Each dimer is well isolated by the $Dy(tta)_2(hfac)$ and $Dy(hfac)_2(tta)$ moieties (ball and stick representation in Figure 4). The shortest intermolecular Dy–Dy distance is equal to 8.578(10) Å (Dy1···Dy2), which is shorter than in 1.

Electrochemical Properties. The redox properties of L and the related complexes 1 and 2 are investigated by cyclic voltammetry (Figure S3 of the Supporting Information), and the values of the oxidation potentials are listed in Table 4.

The cyclic votammogram for L shows two monoelectronic oxidations at ∼0.51 and ∼0.93 V corresponding to the formation of a radical cation and a dication TTF fragment, respectively (Figure S3 of the Supporting Information). These oxidation potentials are the same as those found for the functionalized TTF donor L′,[8a] demonstrating that the nature

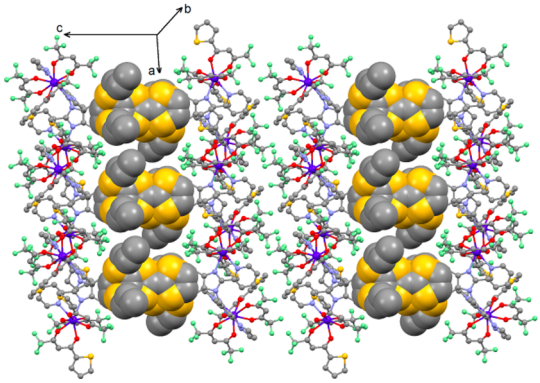

Figure 4. Crystal packing of 2 highlighting the formation of dimers of L.

Table 4. Oxidation Potentials (V vs SCE, nBu_4NPF_6, 0.1 M in CH_2Cl_2 at 100 mV s^{-1}) of Ligand L and Complexes 1 and 2

	$E^1_{1/2}$	$E^2_{1/2}$
L	0.51	0.93
1	0.50	0.94
2	0.48	0.94

of the alkylating group has no influence on the electrochemical properties. Upon coordination of the lanthanide, the electrochemistry does not highlight a significant effect of the electron-attracting $Dy(hfac)_3$, $Dy(hfac)_2(tta)$, and $Dy(hfac)(tta)_2$ fragments on the oxidation potentials (Table 4). The reversibility of the oxidation potentials is conserved, and the electrochemical properties attest to the redox activity of L in the complexes.

Magnetic Properties. *Static Measurements.* The temperature dependencies of $\chi_M T$ for compounds 1 and 2 are shown in Figures S4 and S5 of the Supporting Information. Room-temperature values are slightly smaller (∼27.2 and ∼27.8 cm^3 K mol^{-1} for 1 and 2, respectively) than expected for two isolated ground state multiplets $^6H_{15/2}$ with $g_J = {}^4/_3$ (i.e., 28.4 cm^3 K mol^{-1}).[21] Cooling the sample at 2 K, the thermal depopulation of the ligand-field sublevels leads to a decrease in $\chi_M T$ products. Even if the symmetries of their closest ideal coordination spheres are identical (D_{4d} for Dy1 and D_{3h} for Dy2 in the two compounds), the $\chi_M T$ products at very low temperatures reach different values of 23.1 and 21.8 cm^3 K mol^{-1}, respectively, highlighting both the different electronic distribution of the first neighboring spheres of coordination and the different distortion of the square antiprisms (Table 3). The field dependencies of magnetization measured at 2 K are depicted in the inset of the Figures S4 and S5 of the Supporting Information.

Dynamic Measurements. The out-of-phase components of the ac susceptibility (χ_M'') of 1 and 2 were measured using immobilized powders. They show a frequency dependence in the temperature ranges of 1.8–3.5 and 1.8–14 K for 1 and 2,

DOI: 10.1021/acs.inorgchem.5b00272
Inorg. Chem. 2015, 54, 4021–4028

respectively (external dc field H_{dc} = 0 Oe) (Figure 5 and Figures S6–S9 of the Supporting Information).

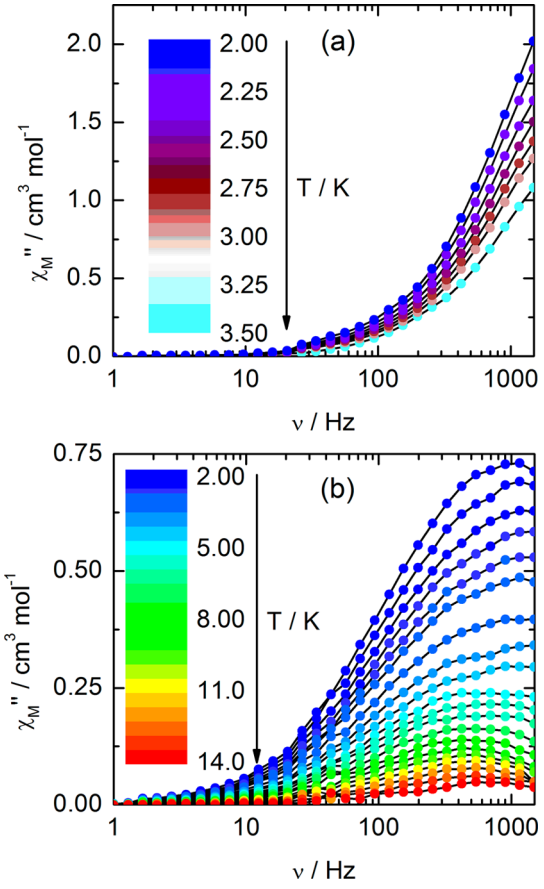

Figure 5. Frequency dependencies of χ_M'' of **1** (a) and **2** (b) in zero field.

The X-ray structures of the compounds revealed two Dy^{III} sites that are expected to present two different dynamic relaxations because the nature and the symmetry of the coordination spheres are rigorously different. By analogy with our previous works, it is known that the Dy^{III} in a N_2O_6 (D_{4d}) environment[8a,b] presents a slow magnetic relaxation, while this is not the case for a Dy^{III} in a N_3O_6 (D_{3h}) environment[13] in zero field. Consequently, the out-of-phase components of the magnetic susceptibility in zero field for **1** and **2** are attributed to the Dy1 site. The absence of a maximum on the χ_M'' versus ν curve for **1** is in agreement with the fact that the substitution of tta^- with $hfac^-$ anions accelerates the relaxation of the Dy^{III} magnetic moment.[8b] To observe maxima on the χ_M'' versus ν curve for **1** and for the Dy2 site, a scan field of the frequency dependence of the magnetic susceptibility was realized and the optimal magnetic fields were extracted (Figure 6). Application of a dc magnetic field shifts the maximum of χ_M'' to a lower frequency, and a second maximum appeared at a high frequency (Figure 6). The optimal applied fields were determined to be equal to 1500 and 3000 Oe for **1** and **2**, respectively. In such applied fields, out-of-phase components of χ_M for **1** and **2** were observed in the temperature range of 2–14 K (Figure 7 and Figures S10 and S11 of the Supporting Information). They displayed a multirelaxation process because two maxima of χ_M'' are observed. This kind of behavior was already observed for both mononuclear and polynuclear

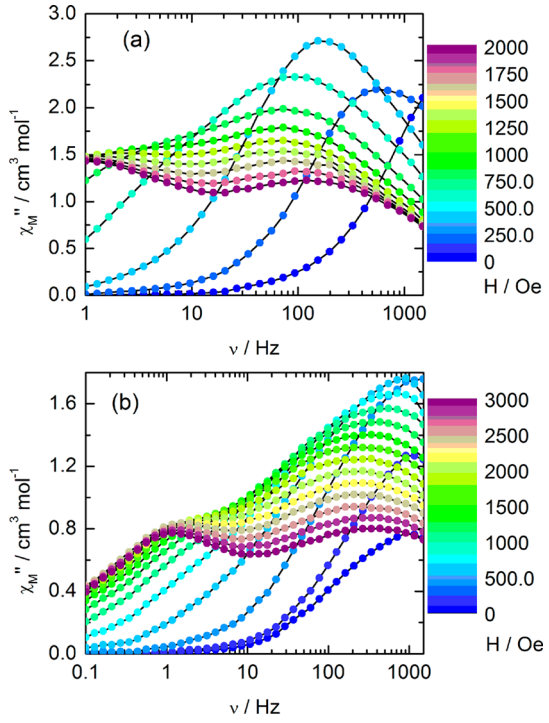

Figure 6. Scan field of the frequency dependence of χ_M'' of **1** (a) and **2** (b) at 2 K.

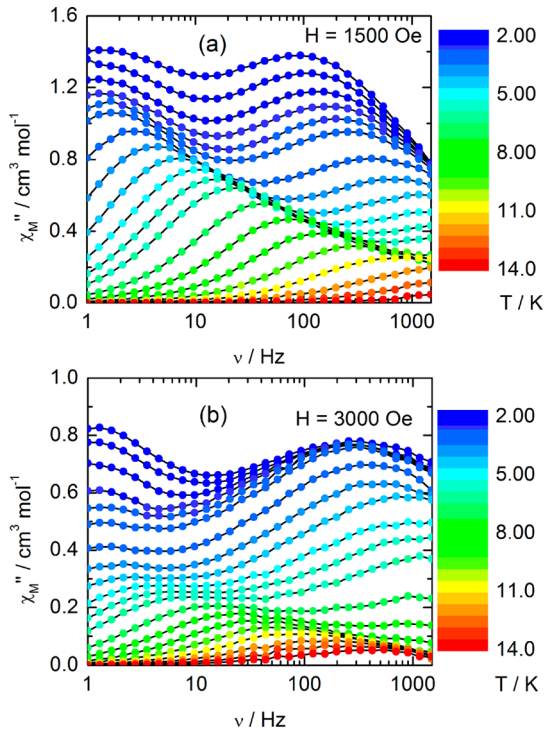

Figure 7. Frequency dependencies of χ_M'' of **1** (a) and **2** (b) in H = 1500 Oe and H = 3000 Oe applied fields, respectively.

complexes. For the mononuclear complexes, the multirelaxation process is observed under an applied magnetic field[8b,3a] and can be attributed to multirelaxation pathways depending of the magnetic field or the presence of different conformers.[22] For polynuclear complexes, the multirelaxation mode can be associated with the SMM behavior at low temperatures and single-ion behavior at higher temperatures[23]

DOI: 10.1021/acs.inorgchem.5b00272
Inorg. Chem. 2015, 54, 4021–4028

or crystallographically different lanthanide ions.[24] In the case presented here, the maxima at low and high frequencies are attributed to the Dy1 and Dy2 sites, respectively, and not to a multirelaxation process associated with one Dy^{III} center.

For both **1** and **2**, an extended Debye model featuring two relaxation times of sites Dy1 and Dy2 was used to treat the ac data in an external dc field. The expressions of χ_M' (**1**) and χ_M'' (**2**) are

$$\chi_M' = \chi_S + (\chi_T - \chi_S)\left\{\frac{\beta\left[1 + (\omega\tau_1)^{1-\alpha_1}\sin\left(\frac{\pi}{2}\alpha_1\right)\right]}{1 + 2(\omega\tau_1)^{1-\alpha_1}\sin\left(\frac{\pi}{2}\alpha_1\right) + (\omega\tau_1)^{2(1-\alpha_1)}} + \frac{(1-\beta)\left[1 + (\omega\tau_2)^{1-\alpha_2}\sin\left(\frac{\pi}{2}\alpha_2\right)\right]}{1 + 2(\omega\tau_2)^{1-\alpha_2}\sin\left(\frac{\pi}{2}\alpha_2\right) + (\omega\tau_2)^{2(1-\alpha_2)}}\right\} \quad (1)$$

$$\chi_M'' = (\chi_T - \chi_S)\left\{\frac{\beta\left[(\omega\tau_1)^{1-\alpha_1}\cos\left(\frac{\pi}{2}\alpha_1\right)\right]}{1 + 2(\omega\tau_1)^{1-\alpha_1}\sin\left(\frac{\pi}{2}\alpha_1\right) + (\omega\tau_1)^{2(1-\alpha_1)}} + \frac{(1-\beta)\left[(\omega\tau_2)^{1-\alpha_2}\cos\left(\frac{\pi}{2}\alpha_2\right)\right]}{1 + 2(\omega\tau_2)^{1-\alpha_2}\sin\left(\frac{\pi}{2}\alpha_2\right) + (\omega\tau_2)^{2(1-\alpha_2)}}\right\} \quad (2)$$

where χ_T and χ_S are the low- and high-frequency limits of susceptibility, respectively, τ_i terms are the relaxation times and α_i terms the distributions of the relaxation time for Dy1 and Dy2 sites, and β is the percentage of the susceptibility relaxing at τ_1. For **1** above 6 K, the two relaxation processes are not separable, so only the relaxation time can be extracted from the experience (Table S1 of the Supporting Information). It must be mentioned that above 11 K the maximum on the χ_M'' versus ν curves are not in the investigated frequency window, so these data are removed from the fitting procedures. Below 6 K, both relaxation times (Table S4 of the Supporting Information) follow a combination of thermally activated and temperature-independent regimes: $\tau^{-1} = \tau_0^{-1}\exp(-\Delta/T) + \tau_{TI}^{-1}$ (where Δ is the energy barrier, τ_0 the relaxation time of the thermally dependent regime, and τ_{TI} the relaxation time of the thermally independent regime) between 2 and 14 K (Figure 8).

The characteristic dynamic parameters of Dy1 and Dy2 in **1** were found to be $\Delta = 18 \pm 0.9$ K, $\tau_0 = (2.15 \pm 0.40) \times 10^{-6}$ s, and $\tau_{TI} = (1.17 \pm 0.09) \times 10^{-3}$ s and $\Delta = 5 \pm 3$ K, $\tau_0 = (1.8 \pm 0.6) \times 10^{-5}$ s, and $\tau_{TI} = 0.14 \pm 0.02$ s, respectively. Interestingly, β is close 50%, which is the value expected if the two Dy1 and Dy2 sites relax with identical static susceptibilities. This assumption can be employed only with caution because low-temperature susceptibility depends on crystal-field splittings that are obviously different in N_2O_6 and N_3O_6. Furthermore, at 1500 Oe, saturation effects must be taken into account. Indeed, the low-temperature value extracted from the extended Debye model is equal to 19.2 cm^3 K mol^{-1}, compared with the value of 23.4 cm^3 K mol^{-1} from dc data. For **2**, as for **1**, only the data below 6 K are reproduced with two relaxation times and with only one above. The characteristic dynamic parameters of Dy1 and Dy2 for **2** (Table S2 of the Supporting Information) were found equal to be $\Delta = 43 \pm 1$ K,

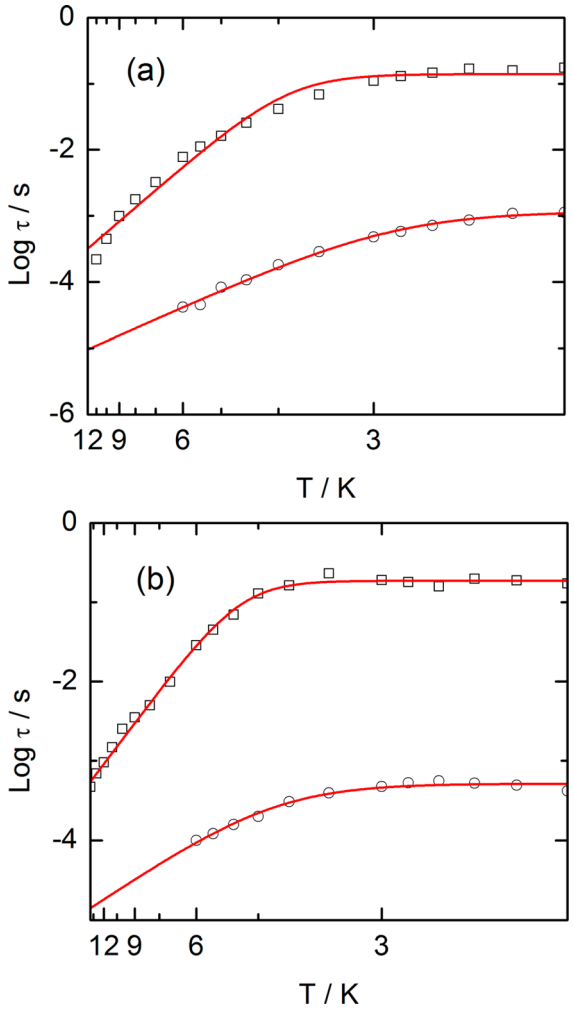

Figure 8. Temperature dependencies of the relaxation times (τ) at 1500 Oe for **1** (a) and 3000 Oe for **2** (b) in the temperature ranges of 2−12 and 2−14 K, respectively. Squares and circles correspond to the data for Dy1 and Dy2 sites, respectively. Black lines are the best-fit curves with modified Arrhenius laws.

$\tau_0 = (2.50 \pm 0.35) \times 10^{-5}$ s, and $\tau_{TI} = 0.19 \pm 0.01$ s and $\Delta = 22 \pm 2$ K, $\tau_0 = (3.05 \pm 1.45) \times 10^{-6}$ s, and $\tau_{TI} = (5.16 \pm 0.25) \times 10^{-4}$ s, respectively. At 3000 Oe, saturation effects dramatically decrease the amplitude of the susceptibility: 12.02 cm^3 K mol^{-1} from ac data at 2 K compared to 21.8 cm^3 K mol^{-1} from dc data. The temperature-independent regime supports the idea that a direct relaxation process between degenerated Kramers doublets of the $^6H_{15/2}$ multiplet operates. The barrier heights of Dy1 are in very good agreement with those measured on Dy^{III}-based mononuclear single-molecule magnets with similar architectures[8a,b] even if in **2** there are only two tta^- anions instead of three in ref 8b.

CONCLUSIONS

Two dinuclear coordination complexes, $[Dy_2(hfac)_6(\mathbf{L})]\cdot(CH_2Cl_2)_2\cdot C_6H_{14}$ (**1**) and $[Dy_2(hfac)_3(tta)_3(\mathbf{L})]$ (**2**), have been synthesized. Their crystalline structures reveal that the two bis-chelating and tris-chelating nitrogenated sites of coordination linked a Dy^{III} ion. In both X-ray structures, Dy1 adopts a square antiprism (D_{4d}) of coordination while Dy2 adopts a spherical tricapped trigonal prism (D_{3h}) of coordination. Interestingly, compound **2** demonstrated that

DOI: 10.1021/acs.inorgchem.5b00272
Inorg. Chem. 2015, 54, 4021−4028

exchange between the ancillary ligand ($hfac^-$ and tta^-) occurred in solution. Both complexes behave as SMM, and the application of an external magnetic field led to a multirelaxation mode. Each mode was attributed to a different Dy^{III} center. The Dy^{III} in a N_2O_6 D_{4d} environment relaxes slower than the Dy^{III} in a N_3O_6 D_{3h} environment. This study shows that it is possible to design ligands with different coordination sites to elaborate molecules incorporating different magnets.

Ligand **L** is chemically suitable for building heterobimetallic 4f4f′ and 3d4f complexes because it involves two radically different sites of coordination with different reactivities and steric hindrance. In particular, additions of physical properties such as luminescence and spin crossover are in progress in our laboratory.

■ ASSOCIATED CONTENT

Supporting Information

Crystallographic information in CIF format, ORTEP views of **1** (Figure S1) and **2** (Figure S2), cyclic voltammetry of **1** and **2** (Figure S3), thermal variation of $\chi_M T$ and first magnetization of **1** (Figure S4) and **2** (Figure S5), temperature dependencies of χ_M' and χ_M'' of **1** (Figure S6) and **2** (Figure S8) in zero field, frequency dependencies of χ_M' and χ_M'' of **1** (Figure S7) and **2** (Figure S9) in zero field, and frequency dependencies of χ_M' and χ_M'' of **1** (Figure S10) and **2** (Figure S11) in an applied field. This material is available free of charge via the Internet at http://pubs.acs.org.

■ AUTHOR INFORMATION

Corresponding Author

*E-mail: fabrice.pointillart@univ-rennes1.fr.

Notes

The authors declare no competing financial interest.

■ ACKNOWLEDGMENTS

This work was supported by the CNRS, Rennes Métropole, Université de Rennes 1, Région Bretagne, FEDER, and Agence Nationale de la Recherche (N° ANR-13-BS07-0022-01).

■ REFERENCES

(1) Woodruff, D. N.; Winpenny, R. E. P.; Layfield, R. A. *Chem. Rev.* **2013**, *113*, 5110−5148.

(2) (a) Gatteschi, D.; Sessoli, R.; Villain, J. *Molecular Nanomagnets*; Oxford University Press: New York, 2006. (b) Bogani, L.; Wernsdorfer, W. *Nat. Mater.* **2008**, *7*, 179−186. (c) Mannini, M.; Pineider, F.; Sainctavit, P.; Danieli, C.; Otero, E.; Sciancalepore, C.; Talarico, A.-M.; Arrio, M.-A.; Cornia, A.; Gatteschi, D.; Sessoli, R. *Nat. Mater.* **2009**, *8*, 194−197. (d) Leuenberger, M. N.; Loss, D. *Nature* **2001**, *410*, 789−793. (e) Lehmann, J.; Gaita-Arino, A.; Coronado, E.; Loss, D. *Nat. Nanotechnol.* **2007**, *2*, 312−317. (f) Ganzhorn, M.; Klyatskaya, S.; Ruben, M.; Wernsdorfer, W. *Nat. Nanotechnol.* **2013**, *8*, 165−169.

(3) (a) Car, P.-E.; Perfetti, M.; Mannini, M.; Favre, A.; Caneschi, A.; Sessoli, R. *Chem. Commun.* **2011**, *47*, 3751−3753. (b) Cucinotta, G.; Perfetti, M.; Luzon, J.; Etienne, M.; Car, P.-E.; Caneschi, A.; Calvez, G.; Bernot, K.; Sessoli, R. *Angew. Chem.* **2012**, *124*, 1638−1642; *Angew. Chem., Int. Ed.* **2012**, *51*, 1606−1610. (c) Boulon, M.-E.; Cucinotta, G.; Luzon, J.; Dedl'Innocenti, C.; Perfetti, M.; Bernot, K.; Calvez, G.; Caneschi, A.; Sessoli, R. *Angew. Chem., Int. Ed.* **2013**, *52*, 350−354.

(4) (a) Jiang, S.-D.; Wang, B.-W.; Su, G.; Wang, Z.-M.; Gao, S. *Angew. Chem.* **2010**, *122*, 7610−7613; *Angew. Chem., Int. Ed.* **2010**, *49*, 7448−7451. (b) Layfield, R. A.; Mcdouall, J. J. W.; Sulway, S. A.; Tuna, F.; Collison, D.; Winpenny, R. E. P. *Chem.—Eur. J.* **2010**, *16*, 4442−4446. (c) Jiang, S.-D.; Liu, S.-S.; Zhou, L.-N.; Wang, B.-W.; Wang, Z.-M.; Gao, S. *Inorg. Chem.* **2012**, *51*, 3079−3087. (d) Jeletic, M.; Lin, P.-H.; Le Roy, J. J.; Korobkov, I.; Gorelsky, S. I.; Murugesu, M. *J. Am. Chem. Soc.* **2011**, *133*, 19286−19289. (e) Demir, S.; Zadrozny, J. M.; Long, J. R. *Chem.—Eur. J.* **2014**, *20*, 9524−9529. (f) Le Roy, J. J.; Jeletic, M.; Gorelsky, S. I.; Korobkov, I.; Ungur, L.; Chibotaru, L. F.; Murugesu, M. *J. Am. Chem. Soc.* **2013**, *135*, 3502−3510.

(5) (a) Ishikawa, N.; Sugita, M.; Ishikawa, T.; Koshihara, S.; Kaizu, Y. *J. Am. Chem. Soc.* **2003**, *125*, 8694−8695. (b) Wang, K.; Zeng, S.; Wang, H.; Doub, J.; Jiang, J. *Inorg. Chem. Front.* **2014**, *1*, 167−171.

(6) Jung, J.; Le Natur, F.; Cador, O.; Pointillart, F.; Calvez, G.; Daiguebonne, C.; Guillou, O.; Guizouarn, T.; Le Guennic, B.; Bernot, K. *Chem. Commun.* **2014**, *50*, 13346−13348.

(7) (a) Wang, Y.; Li, X. L.; Wang, T. W.; Song, Y.; You, X. Z. *Inorg. Chem.* **2010**, *49*, 969−976. (b) Li, D.-P.; Wang, T. W.; Li, C.-H.; Liu, D.-S.; Li, Y.-Z.; You, X.-Z. *Chem. Commun.* **2010**, *46*, 2929−2931. (c) Norel, L.; Bernot, K.; Feng, M.; Roisnel, T.; Caneschi, A.; Sessoli, R.; Rigaut, S. *Chem. Commun.* **2012**, *48*, 3948−3950. (d) Chen, G.-J.; Guo, Y.-N.; Tian, J.-L.; Tang, J.; Gu, W.; Liu, X.; Yan, S.-P.; Cheng, P.; Liao, D.-Z. *Chem.—Eur. J.* **2012**, *18*, 2484−2487. (e) Bi, Y.; Guo, Y.-N.; Zhao, L.; Guo, Y.; Lin, S.-Y.; Jiang, S.-D.; Tang, J.; Wang, B.-W.; Gao, S. *Chem.—Eur. J.* **2011**, *17*, 12476−12481. (f) Wang, Y. L.; Ma, Y.; Yang, X.; Tang, J.; Cheng, P.; Wang, Q.-L.; Li, L.-C.; Liao, D.-Z. *Inorg. Chem.* **2013**, *52*, 7380−7386. (g) Wang, Z.-G.; Lu, J.; Gao, C.-Y.; Wang, C.; Tian, J.-L.; Gu, W.; Liu, X.; Yan, S.-P. *Inorg. Chim. Acta* **2013**, *27*, 127−132.

(8) (a) Cosquer, G.; Pointillart, F.; Golhen, S.; Cador, O.; Ouahab, L. *Chem.—Eur. J.* **2013**, *19*, 7895−7903. (b) da Cunha, T. T.; Jung, J.; Boulon, M.-E.; Campo, G.; Pointillart, F.; Pereira, C. L. M.; Le Guennic, B.; Cador, O.; Bernot, K.; Pineider, F.; Golhen, S.; Ouahab, L. *J. Am. Chem. Soc.* **2013**, *135*, 16332−16335. (c) Pointillart, F.; Bernot, K.; Golhen, S.; Le Guennic, B.; Guizouarn, T.; Ouahab, L.; Cador, O. *Angew. Chem., Int. Ed.* **2015**, *54*, 1504−1507.

(9) (a) Cosquer, G.; Pointillart, F.; Jung, J.; Le Guennic, B.; Golhen, S.; Cador, O.; Guyot, Y.; Brenier, A.; Maury, O.; Ouahab, L. *Eur. J. Inorg. Chem.* **2014**, 69−82. (b) Jung, J.; da Cunha, T. T.; Le Guennic, B.; Pointillart, F.; Pereira, C. L. M.; Luzon, J.; Golhen, S.; Cador, O.; Maury, O.; Ouahab, L. *Eur. J. Inorg. Chem.* **2014**, 3888−3894.

(10) (a) Carbonera, C.; Costa, J. S.; Money, V. A.; Elhaïk, J.; Howard, J. A. K.; Halcrow, M. A.; Létard, J.-F. *Dalton Trans.* **2006**, 3058−3066. (b) Halcrow, M. A. *Coord. Chem. Rev.* **2005**, *249*, 2880−2908. (c) Nihei, M.; Han, L.; Oshio, H. *J. Am. Chem. Soc.* **2007**, *129*, 5312−5313. (d) Rajadurai, C.; Schramm, F.; Fuhr, O.; Ruben, M. *Eur. J. Inorg. Chem.* **2008**, 2649−2653.

(11) (a) Yang, C.; Fu, L.-M.; Wang, Y.; Zhang, J.-P.; Wong, W.-T.; Ai, X.-C.; Qiao, Y.-F.; Zou, B.-S.; Gui, L.-L. *Angew. Chem., Int. Ed.* **2004**, *43*, 5010−5013. (b) Stanley, J. M.; Zhu, X.; Yang, X.; Holliday, B. J. *Inorg. Chem.* **2010**, *49*, 2035−2037. (c) Xue, F.; Ma, Y.; Fu, L.; Hao, R.; Shao, G.; Tang, M.; Zhang, J.; Wang, Y. *Phys. Chem. Chem. Phys.* **2010**, *12*, 3195−3202. (d) Basak, S.; Chandrasekar, R. *Adv. Funct. Mater.* **2011**, *21*, 667−673.

(12) (a) Fu, L.-M.; Wen, X.-F.; Ai, X.-C.; Sun, Y.; Wu, Y.-S.; Zhang, J.-P.; Wang, Y. *Angew. Chem., Int. Ed.* **2005**, *44*, 747−750. (b) Hao, R.; Li, M.; Wang, Y.; Zhang, J.; Ma, Y.; Fu, L.; Wen, X.; Wu, Y.; Ai, X.; Zhang, S.; Wie, Y. *Adv. Funct. Mater.* **2007**, *17*, 3663−3669. (c) Lo, W.-S.; Kwok, W.-M.; Law, G.-L.; Yeung, C.-T.; Chan, C. T.-L.; Yeung, H.-L.; Kong, H.-K.; Chen, C.-H.; Murphy, M.-B.; Wong, K.-L.; Wong, W.-T. *Inorg. Chem.* **2011**, *50*, 5309−5311.

(13) Feng, M.; Pointillart, F.; Le Guennic, B.; Lefeuvre, B.; Golhen, S.; Cador, O.; Maury, O.; Ouahab, L. *Chem.—Asian J.* **2014**, *9*, 2814−2825.

(14) (a) Richardson, M. F.; Wagner, W. F.; Sands, D. E. *J. Inorg. Nucl. Chem.* **1968**, *30*, 1275−1289. (b) Vooshin, A. I.; Shavaleev, N. M.; Kazakov, V. P. *J. Lumin.* **2000**, *91*, 49−58.

(15) Wu, J.; Dupont, N.; Liu, S.-X.; Neels, A.; Hauser, A.; Decurtins, S. *Chem.—Asian J.* **2009**, *4*, 392−399.

(16) (a) Henegar, K. E.; Ashford, S. W.; Baughman, T. A.; Sih, J. C.; Gu, R.-L. *J. Org. Chem.* **1997**, *62*, 6588−6597. (b) Elhaïk; Pask, C. M.; Kilner, C. A.; Halcrow, M. A. *Tetrahedron* **2007**, *63*, 291−298.

DOI: 10.1021/acs.inorgchem.5b00272
Inorg. Chem. 2015, 54, 4021−4028

(17) Sheldrick, G. M. *SHELX97: Programs for Crystal Structure Analysis*, release 97-2; Institüt für Anorganische Chemie der Universität: Göttingen, Germany, 1998. Altomare, A.; Burla, M. C.; Camalli, M.; Cascarano, G. L.; Giacovazzo, C.; Guagliardi, A.; Moliterni, A. G. G.; Polidori, G.; Spagna, R. *J. Appl. Crystallogr.* **1999**, *32*, 115−119.
(18) Petricek, V.; Dusek, M.; Palatinus, L. *JANA, Structure Determination Software Programs*; Institute of Physics: Praha, Czech Republic, 2006.
(19) Spek, A. L. *J. Appl. Crystallogr.* **2003**, *36*, 7−13.
(20) Llunell, M.; Casanova, D.; Cirera, J.; Bofill, J. M.; Alemany, P.; Alvarez, S. *SHAPE*, version 2.1; Barcelona, 2013.
(21) Kahn, O. *Molecular Magnetism*; Wiley-VCH: Weinhem, Germany, 1993.
(22) Jiang, S.-D.; Wang, B.-W.; Sun, H.-L.; Wang, Z.-M.; Gao, S. *J. Am. Chem. Soc.* **2011**, *133*, 4730−4733.
(23) (a) Lin, S.-Y.; Wernsdorfer, W.; Ungur, L.; Powell, A. K.; Guo, Y.-N.; Tang, J.; Zhao, L.; Chibotaru, L. F.; Zhang, H.-J. *Angew. Chem., Int. Ed.* **2012**, *51*, 12767−12771. (b) Blagg, R. J.; Muryn, C. A.; McInnes, E. J. L.; Tuna, F.; Winpenny, R. E. P. *Angew. Chem., Int. Ed.* **2011**, *50*, 6530−6533.
(24) (a) Blagg, R. J.; Ungur, L.; Tuna, F.; Speak, J.; Comar, P.; Collinson, D.; Wernsdorfer, W.; McInnes, E. J. L.; Chibotaru, L. F.; Winpenny, R. E. P. *Nat. Chem.* **2013**, *5*, 673−678. (b) Ruiz, J.; Mota, A. J.; Rodriguez-Diguez, A.; Titos, S.; Herrera, J.-M.; Ruiz, E.; Cremades, E.; Costes, J.-P.; Colacio, E. *Chem. Commun.* **2012**, *48*, 7916−7918. (c) Guo, Y.-N.; Xu, G.-F.; Wernsdorfer, W.; Guo, Y.; Zhang, H.-J. *J. Am. Chem. Soc.* **2011**, *133*, 11948−11951. (d) Venugopal, A.; Tuna, F.; Spaniol, T. R.; Ungur, L.; Chibotaru, L. F.; Okuda, J.; Layfield, R. A. *Chem. Commun.* **2013**, *49*, 901−903. (e) Guo, Y.-N.; Xu, G.-F.; Guo, Y.; Tang, J. *Dalton Trans.* **2011**, *40*, 9953−9963.

DOI: 10.1021/acs.inorgchem.5b00272
Inorg. Chem. 2015, 54, 4021−4028